

# High- $T_c$ superconductivity in weakly electron-doped HfNCl

Betül Pamuk,<sup>1,2</sup> Francesco Mauri,<sup>3,4,\*</sup> and Matteo Calandra<sup>1,†</sup>

<sup>1</sup>CNRS, UMR 7590 and Sorbonne Universités, UPMC Université Paris 06, IMPMC - Institut de Minéralogie, de Physique des Matériaux, et de Cosmochimie, 4 place Jussieu, F-75005 Paris, France

<sup>2</sup>School of Applied and Engineering Physics, Cornell University, Ithaca, New York 14853, USA

<sup>3</sup>Dipartimento di Fisica, Università di Roma La Sapienza, Piazzale Aldo Moro 5, I-00185 Rome, Italy

<sup>4</sup>Graphene Labs, Fondazione Istituto Italiano di Tecnologia, Via Morego, I-16163 Genoa, Italy

(Dated: November 5, 2018)

We investigate the magnetic and superconducting properties in electron-doped  $\text{Li}_x\text{HfNCl}$ .  $\text{HfNCl}$  is a band insulator that undergoes an insulator to superconductor transition upon doping at  $x \approx 0.13$ . The persistence of the insulating state for  $x < 0.13$  is due to an Anderson transition probably related to Li disorder. In the metallic and superconducting phase,  $\text{Li}_x\text{HfNCl}$  is a prototype two-dimensional two-valley electron gas with parabolic bands. By performing a model random phase approximation approach as well as first-principles range-separated Heyd-Scuseria-Ernzerhof (HSE06) calculations, we find that the spin susceptibility  $\chi_s$  is strongly enhanced in the low-doping regime by the electron-electron interaction. Furthermore, in the low-doping limit, the exchange interaction renormalizes the intervalley electron-phonon coupling and results in a strong increase of the superconducting critical temperature for  $x < 0.15$ . On the contrary, for  $x > 0.15$ ,  $T_c$  is approximately constant, in agreement with experiments. At  $x = 0.055$  we found that  $T_c$  can be as large as 40 K, suggesting that the synthesis of cleaner samples of  $\text{Li}_x\text{HfNCl}$  could remove the Anderson insulating state competing with superconductivity and generate a high- $T_c$  superconductor.

PACS numbers: 74.20.Pq, 74.62.Dh, 74.78.-w, 71.10.Ca

## I. INTRODUCTION

The low-doping limit of multivalley semiconductors has recently been proposed as an alternative route to achieve high- $T_c$  superconductivity<sup>1-3</sup>. Transition metal dichalcogenides<sup>4-7</sup>, ternary transition-metal dinitrides<sup>8</sup>, and chloronitrides<sup>9,10</sup> have been reported to achieve fairly high  $T_c$  upon doping. It is possible to dope multivalley semiconductors up to electron densities of  $n \sim 10^{14} \text{ cm}^{-2}$  via field-effect doping<sup>1,4,5,11-13</sup>. The doping of these materials can be also be achieved and controlled by intercalation<sup>9,10,14-17</sup>. However, reaching the low-doping limit can be difficult as disorder and the consequent Anderson transition can suppress superconductivity.

In two-dimensional and quasi-two-dimensional (2D) semiconductors, in the weakly doped regime, the density of states (DOS) is constant. This is different from three-dimensional (3D) semiconductors with parabolic bands, where generally, as the number of electrons increases, the density of states increases as  $\sqrt{\epsilon_F}$ ,  $\epsilon_F$  being the Fermi level. Therefore, in 3D semiconductors, a large number of carriers is needed<sup>18</sup> to achieve a sizable density of states at the Fermi level  $N(0)$ . As in a phonon-mediated mechanism,  $T_c \sim N(0)$ , in a 2D semiconductor,  $T_c$  is expected to be constant because of the constant DOS, as long as the phonon spectrum is weakly affected by doping. However, in the weakly doped regime of transition-metal chloronitrides,  $T_c$  increases with decreasing doping<sup>9,10,14</sup>. This unexpected behavior resulted in a search for a theoretical understanding of the physics of superconductivity in 2D semiconductors<sup>19-26</sup>.

In previous work, it has been shown that in 2D mul-

tivalley semiconductors, at low doping, the electron-electron interaction enhances intervalley electron-phonon coupling, explaining the behavior of  $T_c$ <sup>25,26</sup>. The enhancement of  $T_c$  is linked to the enhancement of the spin susceptibility  $\chi_s$ . Furthermore, a systematic study of the electronic, magnetic, and vibrational properties of  $\text{Li}_x\text{ZrNCl}$  has been performed using density functional theory (DFT) with hybrid functionals with exact exchange and range separation, and this paper shows that the exact exchange component leads to a similar enhancement in spin susceptibility and electron-phonon interaction<sup>26</sup>. This effect on the enhancement of  $T_c$  should be quite general as it only requires basic general ingredients such as a 2D multivalley (ideally two-valley) semiconductor and a large enough electron-gas parameter,  $r_s = 1/a_B\sqrt{\pi n}$  with  $a_B = \epsilon_M\hbar^2/(m^*e^2)$  where  $n$  is the electron density per unit area [linked to the doping per formula unit  $x$  per area  $\Omega$  of 2 formula units (f.u.) for  $\text{Li}_x\text{ZrNCl}$ :  $n = 2x/\Omega$ ],  $\epsilon_M$  is the environmental dielectric constant (i.e., the dielectric constant of the undoped semiconductor), and  $m^*$  the effective mass of the electronic band<sup>25</sup>. Therefore, it is natural to search for high- $T_c$  superconductivity in other materials with either larger  $\epsilon_M$  or with lower  $n$  and  $m^*$ .

An interesting system with these features can be intercalated HfNCl. Superconductivity has been observed with Li-intercalated  $\beta$ -HfNCl with  $T_c = 20 \text{ K}$ <sup>15</sup>, and with co-intercalated  $\text{Li}_{0.48}(\text{THF})_y\text{HfNCl}$  with  $T_c = 25.5 \text{ K}$ <sup>10,15</sup>. As  $\beta$ -ZrNCl,  $\beta$ -HfNCl is a two-dimensional two-valley semiconductor with an almost perfect parabolic conduction band and constant DOS. Moreover, in  $\beta$ -HfNCl,  $\epsilon_M = 4.93$ <sup>21</sup> is slightly smaller than in the case of  $\beta$ -ZrNCl ( $\epsilon_M = 5.59$ ). Thus, it is natural to expect

that a similar enhancement in  $T_c$  at low doping occurs also in  $\text{Li}_x\text{HfNCl}$ . However, the  $T_c$  in  $\text{Li}_x\text{HfNCl}$  is surprisingly flat in the weakly doped regime, and an Anderson transition occurs at almost three times larger doping ( $x \approx 0.15$ ) with respect to  $\text{Li}_x\text{ZrNCl}$ . It is then possible that the Anderson transition prevents the enhancement of  $T_c$  at low doping, or, alternatively, the reported doping is indeed nominal doping and not the real electron doping occurring in the sample. More experimental insight into the low-doping regime can also be obtained by field-effect doping. In this paper, we follow the method introduced in Refs. 25 and 26 to explore the behavior in  $\text{Li}_x\text{HfNCl}$ . We propose that clean samples at sufficiently low doping can achieve higher  $T_c$  without the need of further cointercalation.

## II. COMPUTATIONAL DETAILS

Calculations are performed using the QUANTUM ESPRESSO *ab initio* method<sup>27</sup> with the generalized gradient approximation (GGA) as implemented in the Perdew-Burke-Ernzerhof (PBE) functional<sup>28</sup> with ultrasoft norm conserving pseudopotentials and plane wave basis sets. The doping of the semiconductor is simulated by changing the number of electrons and adding a compensating jellium background, which has been previously shown to give accurate results<sup>20,24</sup>. The atomic coordinates are relaxed with lattice parameters fixed at the experimental values from Ref. 15. For the energy convergence, a threshold on the change in total energy of  $10^{-10}$  Ry is used for all calculations. A Methfessel-Paxton smearing of 0.01 Ry with an electron-momentum grid of  $48 \times 48 \times 48$  are used for the relaxation of the internal coordinates and for calculating the electronic band structure. The density of states is calculated using a Gaussian smearing of 0.01 Ry.

Furthermore, we have performed calculations with the Heyd-Scuseria-Ernzerhof (HSE06)<sup>29</sup> functional that has exact exchange and range separation components, using the CRYSTAL code<sup>30</sup> with Gaussian-type triple- $\zeta$  valence polarized basis set orbitals<sup>31,32</sup>, where the diffuse Gaussian functions of the Hf basis are reoptimized. A Fermi-Dirac smearing of 0.0025 Ha, an electron-momentum grid of  $48 \times 48 \times 16$ , an energy convergence threshold of  $10^{-9}$  Ha, and real space integration tolerances of 8-12-8-30-60, with a sixth order multipolar expansion are used for the HSE06 calculations.

The effective mass  $m^*$  is calculated from the curvature of a fourth order polynomial fit to the region between the Fermi energy and the conduction band minimum around the special point  $\mathbf{K}$ , assuming that the mass tensor is isotropic.

Electron-phonon coupling and phonon frequencies are calculated with the PBE functional with a Methfessel-Paxton smearing of 0.02 Ry, electron-momentum grid of  $12 \times 12 \times 4$ , Wannierization<sup>33</sup> of the electronic bands with an electron-momentum grid of  $6 \times 6 \times 2$ , correspondingly,

a phonon-momentum grid of  $6 \times 6 \times 2$ , and a Wannier interpolation scheme of electron-phonon coupling with a grid of  $40 \times 40 \times 6$ <sup>34</sup>.

## III. RESULTS AND DISCUSSION

### A. Electronic structure

The primitive unit cell of  $\text{HfNCl}$  has rhombohedral structure (space group  $R\bar{3}m$ , No. 166) with 2 f.u. per unit cell. It can also be constructed by a conventional cell of hexagonal structure with 6 f.u. per cell with ABC stacking. Instead of using the rhombohedral unit cell, we take advantage of the weak interlayer interaction<sup>20,24,25,35,36</sup>, which makes the stacking order negligible, and we adopt a hexagonal  $\text{HfNCl}$  structure with AAA stacking. This is equivalent to the hexagonal structure with the space group  $P\bar{3}m1$  (No. 164), with 2 f.u. in the unit cell. We use the experimental lattice parameters  $a$  and  $c$  for each doping from Ref. 15.

To confirm the assumption that the stacking order does not play a significant role in the conduction band, we compare the electronic bands and the density of states of hexagonal and rhombohedral structures for the doping  $x = 0.11$  in Fig. 1. The electronic structure is not affected by the stacking difference.

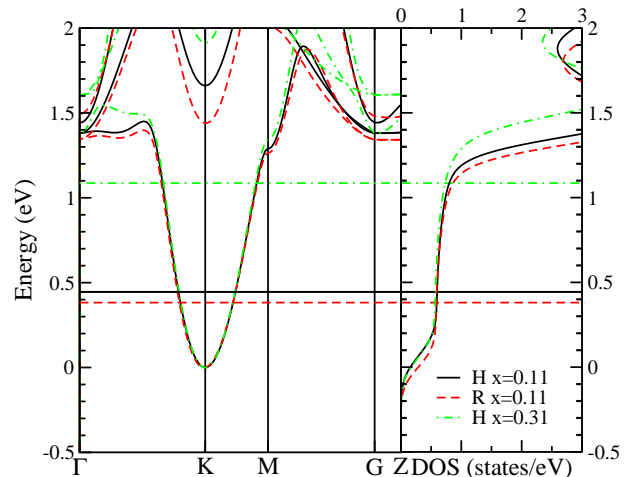


FIG. 1. Electronic structure and density of states (DOS) of  $\text{Li}_x\text{HfNCl}$  calculated with the PBE functional. The hexagonal structure (H) with AAA stacking is compared to the rhombohedral structure (R) with ABC stacking for the doping  $x = 0.11$ . For the hexagonal structure with AAA stacking, the electronic structure of the doping  $x = 0.11$  is compared to that of the doping  $x = 0.31$ . The DOS is given in units of states/eV per 2 f.u. of each unit cell.

This layered system can be considered as the prototype of a 2D two-valley electron gas. Indeed, the bottom of the conduction band of  $\text{HfNCl}$  is composed of two perfectly parabolic bands at points  $\mathbf{K}$  and  $\mathbf{K}' = 2\mathbf{K}$  in the Brillouin zone. The conduction band is a simple parabola,

with a minimum at the  $\mathbf{K}$  point of the Brillouin zone, and the density of states is essentially constant along the parabolic part of the conduction band. The curvature of the rhombohedral structure is slightly smaller, hence the Fermi energy is slightly lower, than the hexagonal structure. This difference also would lead to a slightly larger effective mass calculated with the rhombohedral structure. The rest of the calculations are performed with the hexagonal structure.

Upon Li intercalation, Li atoms are placed between the HfNCl layers. Li acts as a donor and gives electrons to the Hf-N layers. The density of states stays almost constant, as shown in our virtual crystal calculation for  $\text{Li}_x\text{HfNCl}$  in Fig. 1. The semiconducting state is lost with doping and superconductivity emerges. While it is well established that in  $\text{Li}_x\text{ZrNCl}$  the superconducting state is enhanced at low doping<sup>9,10,14</sup>, there is no evidence of this enhancement in experiments with  $\text{Li}_x\text{HfNCl}$ .

TABLE I. The fundamental band gap,  $E_g$  between the valence band maximum at the  $\Gamma$  point and the conduction band minimum at the  $\mathbf{K}$  point, effective mass,  $m^*$ , and density of states at the Fermi level,  $N(0)$  of each doping calculated with the PBE and HSE06 exchange and correlation (XC) functionals with and without exact exchange and range separation.

$x$	XC	$E_g$ (eV)	$m^*$ ( $m_e$ )	$N(0)$ (states/eV)
0	PBE	2.203	0.615	
0.055	PBE	2.195	0.599	0.587
0.11	PBE	2.171	0.585	0.632
0.13	PBE	2.168	0.580	0.639
0.16	PBE	2.164	0.572	0.654
0.18	PBE	2.156	0.568	0.666
0.20	PBE	2.153	0.564	0.680
0.31	PBE	2.130	0.540	0.833
0	HSE06	3.330	0.522	
0.055	HSE06	3.240	0.496	0.511
0.11	HSE06	3.148	0.472	0.539
0.13	HSE06	3.121	0.466	0.545
0.16	HSE06	3.084	0.456	0.556
0.18	HSE06	3.055	0.451	0.565
0.20	HSE06	3.031	0.446	0.577
0.31	HSE06	2.908	0.425	0.723

In Table I, we present the band gap  $E_g$ , effective mass  $m^*$ , and density of states  $N(0)$  of each doping with the PBE and HSE06 functionals. The band gap  $E_g$  decreases with increased doping for both functionals. As the doping increases, the  $m^*$  decreases, and this trend is similar in  $\text{ZrNCl}$ <sup>26</sup>. However, in general, the effective mass of HfNCl is slightly larger than that of ZrNCl. Similarly,  $N(0)$  is larger in HfNCl than ZrNCl for all doping<sup>26</sup>.

## B. Spin susceptibility

Similar to  $T_c$ , the magnetic spin susceptibility is enhanced in  $\text{Li}_x\text{ZrNCl}$  at low doping<sup>37,38</sup>, whereas there are no experiments of spin susceptibility as a function of doping for  $\text{Li}_x\text{HfNCl}$ . Spin susceptibility is the response

of the spin magnetization to an applied magnetic field,

$$\chi_s = \left( \frac{\partial^2 E}{\partial M^2} \right)^{-1}, \quad (1)$$

where  $E$  and  $M$  are the total energy and magnetization, respectively. The noninteracting spin susceptibility  $\chi_{0s}$  is obtained by neglecting the electron-electron interaction of the conducting electrons. For perfectly parabolic bands, the noninteracting spin susceptibility is doping independent and equal to

$$\chi_{0s} = \mu_s N(0) = \frac{g_v m^*}{\pi \hbar^2}, \quad (2)$$

where  $\mu_s$  is the Bohr magneton,  $g_v$  is the valley degeneracy (2 in our case), and  $m^*$  the band effective mass. We calculate  $\chi_{0s}$  from the density of states of the undoped compound, and by extrapolating  $N(0)$  of the desired doping. Our calculations show that  $\chi_{0s}$  is not enhanced at the low-doping limit. As  $N(0)$  is larger in HfNCl,  $\chi_{0s}$  is also larger in HfNCl than ZrNCl<sup>26</sup>.

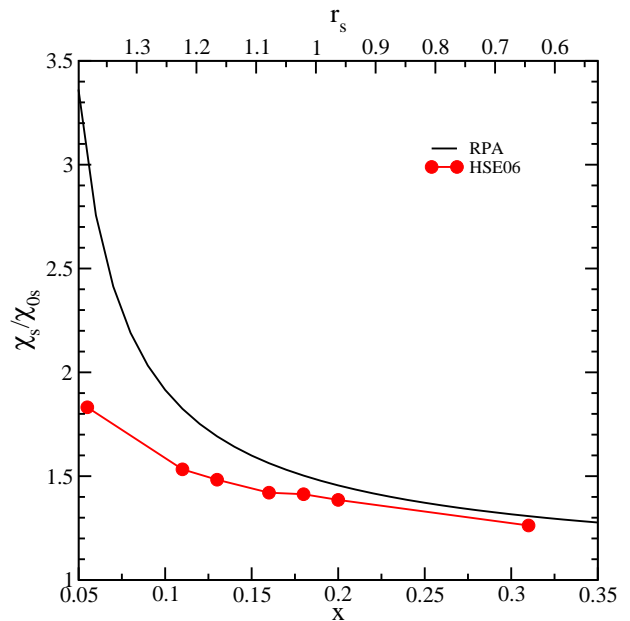


FIG. 2. Spin susceptibility enhancement at different doping with the RPA and HSE06 approximations.

We calculate the spin susceptibility with the HSE06 hybrid functional by calculating the total energy at fixed magnetization and then using equation 1 to obtain  $\chi_s$ . We choose the HSE06 functional, because it can reproduce the  $\chi_s/\chi_{0s}$  of ZrNCl<sup>26</sup>. We also compare our results with those obtained by a model based on the random phase approximation (RPA)<sup>25,39</sup>. The model is appropriate in the low-doping limit where  $|\mathbf{k}_F - \mathbf{K}| \ll K$ , a condition necessary to have the intravalley electron-electron scattering dominating over the intervalley one, as explained in the Supplemental Material of Ref. 25. This model assumes a 2D two-valley electron gas with

no intervalley Coulomb scattering. Therefore, only the intravalley electron-electron interaction remains and the RPA susceptibility can be calculated analytically, by using the PBE effective mass of undoped HfNCl and the environmental dielectric constant  $\epsilon_M = 4.93^{21}$ . This value is smaller in HfNCl than ZrNCl ( $\epsilon_M = 5.59$ )<sup>25</sup>.

In a 2D two-valley electron gas, the reduction of doping implies an increase of the  $r_s$  electron-gas parameter, and, consequently, of the electron-electron interaction<sup>40</sup>. The effective mass of  $\beta$ -HfNCl as calculated by the PBE functional is larger ( $0.615 m_e$ ) than  $\beta$ -ZrNCl ( $0.57 m_e$ )<sup>25</sup>. Therefore, both the larger  $m^*$  and the smaller  $\epsilon_M$  of HfNCl lead to larger  $r_s$ , as compared to ZrNCl, at a similar low-doping regime<sup>25</sup>. This implies that the electron-electron interaction is larger in HfNCl, and hence the spin susceptibility enhancement is also larger in HfNCl. While the spin susceptibility enhancement at low doping is present for both calculations with the RPA and the HSE06 functional, as presented in Fig. 2, it is milder with the HSE06 functional than the RPA calculation.

### C. Electron-phonon interaction

The electron-phonon coupling of a mode  $\nu$  at a phonon momentum  $\mathbf{q}$  is defined as

$$\tilde{\lambda}_{\mathbf{q}\nu} = \frac{2}{\omega_{\mathbf{q}\nu}^2 N(0) N_k} \sum_k |\tilde{d}_{\mathbf{k},\mathbf{k}+\mathbf{q}}^\nu|^2 \delta(\epsilon_{\mathbf{k}}) \delta(\epsilon_{\mathbf{k}+\mathbf{q}}), \quad (3)$$

where  $\epsilon_{\mathbf{k}}$  is the quasiparticle energy and the electron-phonon matrix elements are defined such that  $\tilde{d}_{\mathbf{k},\mathbf{k}+\mathbf{q}}^\nu = \langle \mathbf{k} | \delta \tilde{V} / \delta u_{\mathbf{q}\nu} | \mathbf{k} + \mathbf{q} \rangle$ ,  $u_{\mathbf{q}\nu}$  is the phonon displacement of the mode  $\omega_{\mathbf{q}\nu}$ , and  $\tilde{V}$  is the single particle potential that is fully screened by charge, spin, and valley exchange and correlation effects [see Eq. (2) in Ref. 25 for more details]. We first calculate the noninteracting  $\lambda_{\mathbf{q}\nu}$  with the PBE functional, which does not have valley polarization dependence, using the Wannier interpolation method<sup>34</sup>.

In Fig. 3, we show the phonon dispersion along the high symmetry directions, and the Eliashberg function  $\alpha^2 F(\omega)$  and the electron-phonon coupling  $\lambda(\omega)$  for the doping  $x = 0.055$ . The Eliashberg function has two distinct peaks that are dominated by the modes with large phonon linewidths  $\gamma_{\mathbf{q}\nu}$  at the  $\mathbf{K}$  point of the Brillouin zone at the energies  $\sim 19$  meV and  $\sim 59$  meV. To analyze the contribution to the electron-phonon coupling, we separate it into the inter- and intra-valley components. The intervalley electron-phonon coupling  $\lambda^{\text{inter}}$  is defined such that the modes contributing to the coupling are in the vicinity of the  $\mathbf{K}$  and  $2\mathbf{K}$  points such that, in Eq. (3),  $\mathbf{k} \in I(\mathbf{K})$  and  $\mathbf{k} + \mathbf{q} \in I(2\mathbf{K})$ ; or  $\mathbf{k} \in I(2\mathbf{K})$  and  $\mathbf{k} + \mathbf{q} \in I(\mathbf{K})$ . The rest of the coupling is attributed to the intravalley electron-phonon coupling  $\lambda^{\text{intra}}$ . Also shown in Fig. 3 is that these modes at the  $\mathbf{K}$  point contribute significantly to the intervalley component of the Eliashberg function and have a large intervalley electron-phonon coupling  $\lambda^{\text{inter}}$ . Therefore, they induce a valley polarization in this system<sup>25</sup>.

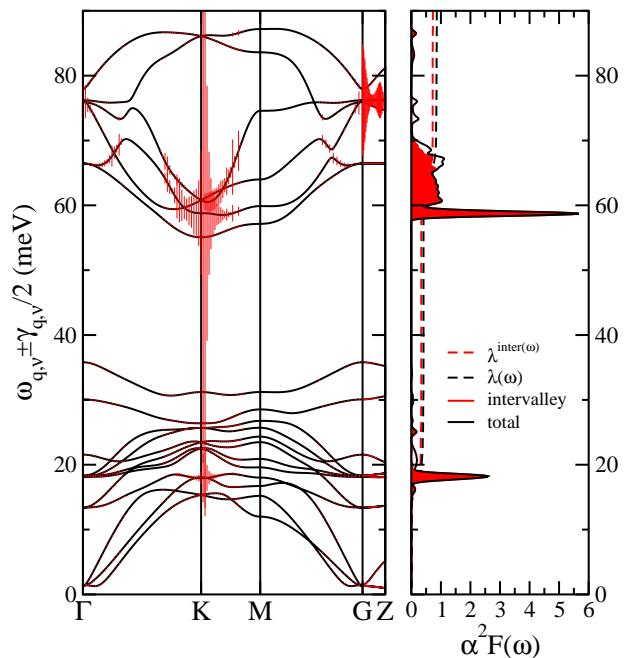


FIG. 3. Left: Phonon dispersion along the high symmetry directions of the Brillouin zone for  $\text{Li}_{0.055}\text{HfNCl}$ . Right: The total and intervalley component of the Eliashberg function  $\alpha^2 F(\omega)$  and the electron-phonon coupling  $\lambda(\omega)$ .

Consequently, the spin susceptibility enhancement is directly linked to the enhancement in the electron-phonon coupling due to the intervalley interaction<sup>25,26</sup>. The intervalley electron-phonon coupling is enhanced similarly to  $\chi_s/\chi_{0s}$  such that

$$\frac{\tilde{\lambda}_{\mathbf{q}\nu}^{\text{inter}}}{\lambda_{\mathbf{q}\nu}^{\text{inter}}} = \left( \frac{\chi_s}{\chi_{s0}} \right)^2. \quad (4)$$

Following the previously developed methodology,<sup>25,26</sup> we first calculate the bare intervalley electron-phonon coupling  $\lambda$  with the PBE functional, and use the spin susceptibility enhancement of RPA or HSE06 to obtain the corresponding fully dressed coupling  $\tilde{\lambda}$ .

In Table II, we present the bare electron-phonon coupling  $\lambda$ , and its intra- and intervalley components,  $\lambda^{\text{intra}}$ ,  $\lambda^{\text{inter}}$  calculated with the PBE functional, as well as the fully interacting electron-phonon coupling for the RPA and the HSE06 calculations,  $\tilde{\lambda}^{\text{RPA}}$ ,  $\tilde{\lambda}^{\text{HSE06}}$  and their corresponding  $\omega_{\text{log}}$  values.

### D. Superconductivity and $T_c$ enhancement

Finally, we calculate the superconducting critical temperature  $T_c$  using the McMillan-Allen-Dynes equation<sup>41,42</sup>,

$$T_c = \frac{\omega_{\text{log}}}{1.20} \exp \left( -\frac{1.04(1 + \tilde{\lambda})}{\tilde{\lambda} - \mu^*(1 + 0.62\tilde{\lambda})} \right), \quad (5)$$

TABLE II. For each doping, bare electron-phonon coupling  $\lambda$  and its intravalley  $\lambda^{\text{intra}}$  and intervalley  $\lambda^{\text{inter}}$  components as calculated by the PBE functional; fully interacting electron-phonon coupling for the RPA and the HSE06 functionals  $\tilde{\lambda}^{\text{RPA}}$  and  $\tilde{\lambda}^{\text{HSE06}}$ ; PBE functional values of  $\omega_{\log}^{\text{PBE}}$  with intra- and intervalley components  $\omega_{\log}^{\text{PBEintra}}$  and  $\omega_{\log}^{\text{PBEinter}}$ ; and rescaled  $\omega_{\log}^{\text{RPA}}$  and  $\omega_{\log}^{\text{HSE06}}$  in meV. The screened Coulomb pseudopotential  $\mu^*$  and the  $T_c$  values calculated by the RPA and HSE06 functional are also given.

$x$	$\lambda$	$\lambda^{\text{intra}}$	$\lambda^{\text{inter}}$	$\tilde{\lambda}^{\text{RPA}}$	$\tilde{\lambda}^{\text{HSE06}}$	$\omega_{\log}^{\text{PBE}}$	$\omega_{\log}^{\text{PBEintra}}$	$\omega_{\log}^{\text{PBEinter}}$	$\omega_{\log}^{\text{RPA}}$	$\omega_{\log}^{\text{HSE06}}$	$\mu^*$	$T_c^{\text{RPA}}$	$T_c^{\text{HSE06}}$
0.055	0.861	0.133	0.728	6.730	2.578	34.219	28.494	35.385	35.233	34.991	0.326	68.60	39.39
0.11	0.789	0.167	0.622	2.236	1.628	32.593	28.285	33.854	33.404	33.235	0.276	38.15	25.18
0.13	0.803	0.182	0.621	1.959	1.547	31.458	27.882	32.588	32.120	31.997	0.266	32.97	23.36
0.16	0.860	0.208	0.652	1.800	1.523	28.643	26.451	29.380	29.026	28.962	0.254	28.17	21.86
0.18	0.889	0.225	0.664	1.724	1.551	26.781	25.103	27.373	27.066	27.032	0.248	25.69	21.67
0.20	0.932	0.256	0.676	1.688	1.554	26.370	24.686	27.040	26.668	26.636	0.242	24.81	21.96
0.31	0.973	0.372	0.601	1.401	1.331	25.915	25.956	25.887	25.905	25.906	0.222	19.89	18.30

where  $\mu^* = \mu/[1 + \mu \log(\epsilon_F/\omega_D)]$  is the screened Coulomb pseudopotential, with  $\epsilon_F$  and  $\omega_D = 900$  meV being the Fermi and Debye energy, respectively. We set the unscreened  $\mu = 0.231$  that gives the correct estimate of the experimental  $T_c = 19.94$  K at the highest doping of  $x = 0.31$  by using the RPA enhanced fully screened electron-phonon coupling  $\tilde{\lambda}$ . This is in agreement with the GW estimate of  $\mu = 0.237$  at  $x = 0.1$ <sup>22</sup>. We present the screened Coulomb pseudopotential  $\mu^*$  that is used to calculate  $T_c$  for each doping and the final  $T_c$  values for the RPA and HSE06 calculations in Table II.

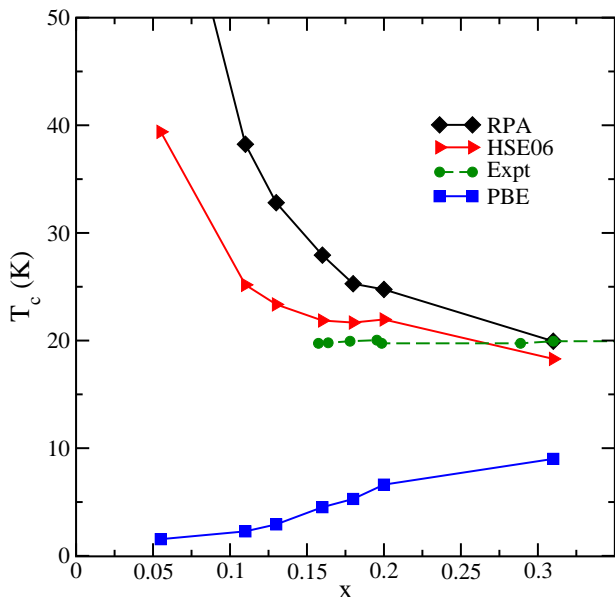


FIG. 4. Superconducting critical temperature  $T_c$  as a function of doping calculated with the bare electron-phonon coupling  $\lambda_{q\nu}$  as calculated by the PBE functional, and with fully dressed electron-phonon coupling,  $\tilde{\lambda}_{q\nu}$  using the RPA and HSE06 functional. The experimental data are taken from Ref. 15.

With the PBE functional, the superconducting temperature,  $T_c$  is reduced in the low-doping limit, in stark disagreement with experiments, as shown in Fig. 4. When the dressing of the intervalley electron-phonon

coupling by the intravalley Coulomb interaction is taken into account,  $T_c$  is enhanced in a similar fashion to what happens to the spin susceptibility, i.e., it is enhanced significantly, up to  $\sim 70$  K, with RPA, while the enhancement is softer, up to  $\sim 40$  K with the HSE06 functional. In addition, the HSE06 functional agrees well with the experimental  $T_c$  for the doping between  $0.15 < x < 0.20$ . We show the details of this scaling for the RPA calculation in Appendix A, and we present the phonon dispersion,  $\omega$ , Eliashberg function  $\alpha^2F(\omega)$ , and electron-phonon coupling  $\lambda(\omega)$  for the rest of the dopings in Appendix B.

#### IV. CONCLUSION

We study the electronic, magnetic, and vibrational properties of  $\text{Li}_x\text{HfNCl}$  at the low-doping regime. We first calculate the electronic structure and find that the effective mass  $m^*$  and the density of states  $N(0)$  are larger in  $\text{HfNCl}$  as compared to  $\text{ZrNCl}$ , both for the PBE and the HSE06 functionals.

As there are no experimental data for the spin susceptibility of  $\text{HfNCl}$  as a function of doping, we calculate the spin susceptibility enhancement using both RPA calculations and the HSE06 functional. Both  $m^*$  and  $\epsilon_M$  contribute to a larger  $r_s$  in  $\text{HfNCl}$  than  $\text{ZrNCl}$ . Therefore, spin susceptibility enhancement is larger in  $\text{HfNCl}$  than  $\text{ZrNCl}$  at the low-doping limit, and this is visible both in the RPA calculations and the HSE06 calculations of  $\chi_s/\chi_{0s}$ .

Then, we calculate the phonon dispersion  $\omega_{q\nu}$ , Eliashberg function  $\alpha^2F(\omega)$ , and the bare electron-phonon coupling  $\lambda(\omega)$  using the PBE functional. We further calculate the fully-dressed electron-phonon coupling  $\tilde{\lambda}$ , based on the enhancement in the spin susceptibility.

This enhancement is then directly reflected in the calculated  $T_c$ . There is no enhancement in  $T_c$  with the PBE functional. On the other hand, we can speculate that depending on the enhancement in the spin susceptibility, high  $T_c$  can be reached, ranging from 40 K (with the HSE06 functional) to 70 K (with the RPA calculation). Furthermore, the HSE06 functional gives comparable  $T_c$

values to the experiments for dopings  $0.15 < x < 0.20$ . However, the  $T_c$  goes to zero in experiments for the reported doping  $x < 0.15$ <sup>15</sup>. A possible explanation for this disagreement is that the disorder at the low-doping limit can lead to Anderson localization. Alternatively, it could be that the reported doping is only a nominal doping. Experiments on field-effect doping can also help one to learn more about the low-doping regime. In either case, our results predict that the removal of the Anderson transition or better control of doping in  $\text{Li}_x\text{HfNCI}$  could lead to the emergence of a high- $T_c$  superconducting state.

## ACKNOWLEDGMENTS

This project has received funding from the Graphene Flagship by the European Union's Horizon 2020 research and innovation programme under Grant Agreement No. 696656 GrapheneCore1. We acknowledge PRACE for awarding us access to resource on Marenostrum at BSC based in Spain; and the computer facilities provided by CINES, IDRIS, CEA TGCC (Grant EDARI No. 2017091202), and institute for computing and data sciences (ISCD) at UPMC based in France. B.P. acknowledges National Science Foundation [Platform for the Accelerated Realization, Analysis, and Discovery of Interface Materials (PARADIM)] under Cooperative Agreement No. DMR-1539918 for her time at Cornell University.

## Appendix A: Electron-phonon Coupling Scaling

We present the electron-phonon coupling in Eq. (5) as a function of doping in Fig. 5. The top panel shows the average noninteracting electron-phonon coupling  $\lambda$ , as well as its inter- and intravalley components.

The second panel shows the total  $\omega_{\log}$ , also decomposed into inter- and intravalley components. In addition, we also present how it is rescaled with the RPA calculation, by rescaling  $\tilde{\lambda}_{\text{inter}}$ . Starting with the definition of  $\omega_{\log}$ ,

$$\omega_{\log} = \exp \left[ \frac{2}{\lambda} \int_0^{+\infty} \alpha^2 F(\omega) \frac{\log(\omega)}{\omega} d\omega \right], \quad (\text{A1})$$

we have separated  $\omega_{\log}$  into inter- and intravalley terms. The intervalley term is

$$\omega_{\log}^{\text{inter}} = \exp \left[ \frac{2}{\lambda^{\text{inter}}} \int_0^{+\infty} \alpha^2 F(\omega)^{\text{inter}} \frac{\log(\omega)}{\omega} d\omega \right], \quad (\text{A2})$$

and the intravalley term is defined similarly. The relation between these two terms hold such that

$$\omega_{\log} = (\omega_{\log}^{\text{inter}})^{\lambda^{\text{inter}}/\lambda} \times (\omega_{\log}^{\text{intra}})^{\lambda^{\text{intra}}/\lambda}. \quad (\text{A3})$$

Therefore, we rescaled it for the RPA calculation by keeping the intravalley  $\lambda^{\text{intra}}$  component the same, but rescaling the fully interacting intervalley  $\tilde{\lambda}^{\text{inter}}$  and hence the

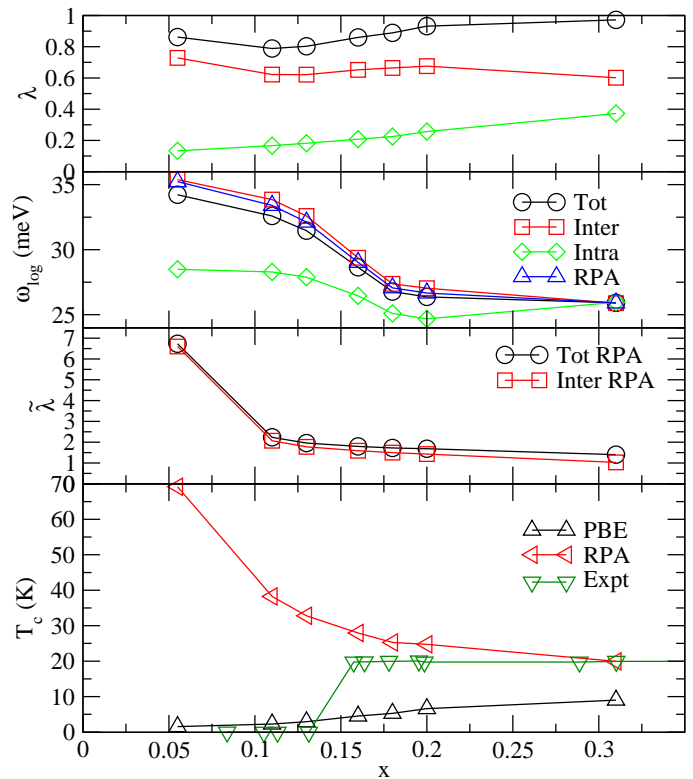


FIG. 5. First panel: Average noninteracting electron-phonon coupling  $\lambda$  for each doping including the inter- and intravalley components as calculated with the PBE functional. Second panel:  $\omega_{\log}$  for each doping with inter- and intravalley components, as well as rescaled  $\omega_{\log}^{\text{RPA}}$ . Third panel: Interacting electron-phonon coupling  $\tilde{\lambda}$  where the intervalley term is rescaled with RPA electron-electron interaction enhancement. Fourth panel: Superconducting critical temperature  $T_c$  as a function of doping, calculated by noninteracting (PBE) and interacting (RPA) electron-phonon coupling, as compared to the experiments from Ref. 15.

total  $\tilde{\lambda}$  electron-phonon coupling elements. These are shown in the third panel of the figure for the RPA calculations.

For completeness, we also present the final calculated  $T_c$  without an intervalley enhancement using the PBE functional, and with an intervalley enhancement using the RPA calculation, similar to Fig. 4.

## Appendix B: Phonon Modes as a Function of Doping

In this Appendix, we present the phonon dispersion of  $\text{Li}_x\text{HfNCI}$  for all doping values. The left panels of Fig. 6 show the phonon dispersion with increasing doping. Similarly the right panels show the corresponding Eliashberg function  $\alpha^2 F(\omega)$  and the electron-phonon coupling  $\lambda(\omega)$ . In all cases, there are two distinct peaks of  $\alpha^2 F(\omega)$ , and consequently an increase in the  $\lambda(\omega)$ .

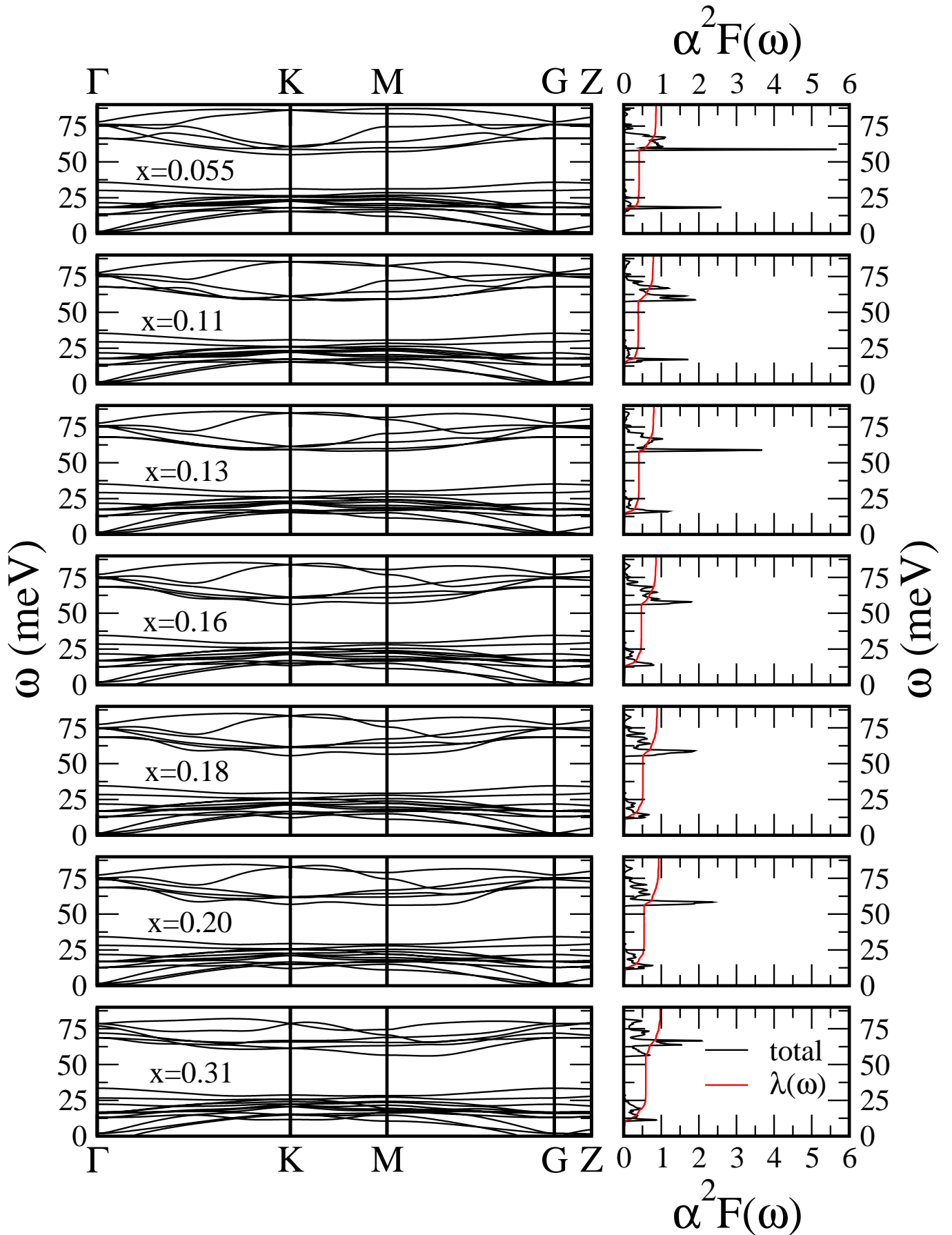


FIG. 6. Left: Phonon dispersion of  $\text{Li}_x\text{HfNCl}$  as a function of doping. Right: Total Eliashberg function  $\alpha^2 F(\omega)$  and electron-phonon coupling  $\lambda(\omega)$ .

- \* francesco.mauri@uniroma1.it  
† matteo.calandra@upmc.fr
- <sup>1</sup> Y. Saito, Y. Kasahara, J. Ye, Y. Iwasa, and T. Nojima, *Science* **350**, 409 (2015).
  - <sup>2</sup> J. M. Lu, O. Zheliuk, I. Leermakers, N. F. Q. Yuan, U. Zeitler, K. T. Law, and J. T. Ye, *Science* **350**, 1353 (2015).
  - <sup>3</sup> Y. Kasahara, K. Kuroki, S. Yamanaka, and Y. Taguchi, *Physica C: Superconductivity and its Applications* **514**, 354 (2015).
  - <sup>4</sup> K. S. Novoselov, D. Jiang, F. Schedin, T. J. Booth, V. Khotkevich, S. V. Morozov, and A. K. Geim, *Proc. Nat. Acc. Sci.* **102**, 10451 (2005).
  - <sup>5</sup> X. Xu, W. Yao, D. Xiao, and T.-F. Heinz, *Nat. Phys.* **10**, 343 (2014).
  - <sup>6</sup> Y. J. Zhang, T. Oka, R. Suzuki, J. T. Ye, and Y. Iwasa, *Science* **344**, 725 (2014).
  - <sup>7</sup> J. T. Ye, Y. J. Zhang, R. Akashi, M. S. Bahramy, R. Arita, and Y. Iwasa, *Science* **338**, 1193 (2012).
  - <sup>8</sup> D. Gregory, M. Barker, P. Edwards, M. Slaskic, and D. Siddonsa, *J. Solid State Chem.* **137**, 62 (1998).
  - <sup>9</sup> S. Yamanaka, H. Kawaji, K. i. Hotehama, and M. Ohashi, *Adv. Mater.* **8**, 771 (1996).
  - <sup>10</sup> S. Yamanaka, K. Hotehama, and H. Kawaji, *Nature (London)* **392**, 580 (1998).
  - <sup>11</sup> J. T. Ye, S. Inoue, K. Kobayashi, Y. Kasahara, H. T. Yuan, H. Shimotani, and Y. Iwasa, *Nat. Mater.* **9**, 125 (2010).
  - <sup>12</sup> Y. Kasahara, T. Nishijima, T. Sato, Y. Takeuchi, J. Ye, H. Yuan, H. Shimotani, and Y. Iwasa, *J. Phys. Soc. Jpn.* **80**, 023708 (2011).
  - <sup>13</sup> T. Brumme, M. Calandra, and F. Mauri, *Phys. Rev. B* **89**, 245406 (2014).
  - <sup>14</sup> Y. Taguchi, A. Kitora, and Y. Iwasa, *Phys. Rev. Lett.* **97**, 107001 (2006).
  - <sup>15</sup> T. Takano, T. Kishiume, Y. Taguchi, and Y. Iwasa, *Phys. Rev. Lett.* **100**, 247005 (2008).
  - <sup>16</sup> T. Takano, A. Kitora, Y. Taguchi, and Y. Iwasa, *Journal of Physics and Chemistry of Solids* **69**, 3089 (2008).
  - <sup>17</sup> S. Yamanaka, T. Yasunaga, K. Yamaguchi, and M. Tagawa, *J. Mater. Chem.* **19**, 2573 (2009).
  - <sup>18</sup> E. A. Ekimov, V. A. Sidorov, E. D. Bauer, N. N. Mel'nik, N. J. Curro, J. D. Thompson, and S. M. Stishov, *Nature (London)* **428**, 542 (2004).
  - <sup>19</sup> R. Weht, A. Filippetti, and W. E. Pickett, *Europhys. Lett.* **48**, 320 (1999).
  - <sup>20</sup> R. Heid and K.-P. Bohnen, *Phys. Rev. B* **72**, 134527 (2005).
  - <sup>21</sup> A. Kaur, E. R. Ylvisaker, Y. Li, G. Galli, and W. E. Pickett, *Phys. Rev. B* **82**, 155125 (2010).
  - <sup>22</sup> R. Akashi, K. Nakamura, R. Arita, and M. Imada, *Phys. Rev. B* **86**, 054513 (2012).
  - <sup>23</sup> Z. P. Yin, A. Kutepov, and G. Kotliar, *Phys. Rev. X* **3**, 021011 (2013).
  - <sup>24</sup> A. S. Botana and W. E. Pickett, *Phys. Rev. B* **90**, 125145 (2014).
  - <sup>25</sup> M. Calandra, P. Zocante, and F. Mauri, *Phys. Rev. Lett.* **114**, 077001 (2015).
  - <sup>26</sup> B. Pamuk, J. Baima, R. Dovesi, M. Calandra, and F. Mauri, *Phys. Rev. B* **94**, 035101 (2016).
  - <sup>27</sup> P. Giannozzi, S. Baroni, N. Bonini, M. Calandra, R. Car, C. Cavazzoni, D. Ceresoli, G. L. Chiarotti, M. Cococcioni, I. Dabo, A. Dal Corso, S. de Gironcoli, S. Fabris, G. Fratesi, R. Gebauer, U. Gerstmann, C. Gougousis, A. Kokalj, M. Lazzeri, L. Martin-Samos, N. Marzari, F. Mauri, R. Mazzarello, S. Paolini, A. Pasquarello, L. Paulatto, C. Sbraccia, S. Scandolo, G. Sclauzero, A. P. Seitsonen, A. Smogunov, P. Umari, and R. M. Wentzcovitch, *J. Phys. Condens. Matter* **21**, 395502 (2009).
  - <sup>28</sup> J. P. Perdew, K. Burke, and M. Ernzerhof, *Phys. Rev. Lett.* **77**, 3865 (1996).
  - <sup>29</sup> A. V. Krukau, O. A. Vydrov, A. F. Izmaylov, and G. E. Scuseria, *J. Chem. Phys.* **125**, 224106 (2006).
  - <sup>30</sup> R. Dovesi, R. Orlando, A. Erba, C. M. Zicovich-Wilson, B. Civalieri, S. Casassa, L. Maschio, M. Ferrabone, M. D. L. Pierre, P. D'Arco, Y. Noël, M. Causà, M. Rérat, and B. Kirtman, *Int. J. Quantum Chem.* **114**, 1287 (2014).
  - <sup>31</sup> F. Weigend and R. Ahlrichs, *Phys. Chem. Chem. Phys.* **7**, 3297 (2005).
  - <sup>32</sup> D. Muñoz Ramo, J. L. Gavartin, A. L. Shluger, and G. Bersuker, *Phys. Rev. B* **75**, 205336 (2007).
  - <sup>33</sup> A. A. Mostofi, J. R. Yates, G. Pizzi, Y.-S. Lee, I. Souza, D. Vanderbilt, and N. Marzari, *Computer Physics Communications* **185**, 2309 (2014).
  - <sup>34</sup> M. Calandra, G. Profeta, and F. Mauri, *Phys. Rev. B* **82**, 165111 (2010).
  - <sup>35</sup> Y. Kasahara, T. Kishiume, K. Kobayashi, Y. Taguchi, and Y. Iwasa, *Phys. Rev. B* **82**, 054504 (2010).
  - <sup>36</sup> T. Takano, Y. Kasahara, T. Oguchi, I. Hase, Y. Taguchi, and Y. Iwasa, *J. Phys. Soc. Jpn.* **80**, 023702 (2011).
  - <sup>37</sup> Y. Kasahara, T. Kishiume, T. Takano, K. Kobayashi, E. Matsuoka, H. Onodera, K. Kuroki, Y. Taguchi, and Y. Iwasa, *Phys. Rev. Lett.* **103**, 077004 (2009).
  - <sup>38</sup> Y. Taguchi, Y. Kasahara, T. Kishiume, T. Takano, K. Kobayashi, E. Matsuoka, H. Onodera, K. Kuroki, and Y. Iwasa, *Physica C: Superconductivity* **470**, S598 (2010).
  - <sup>39</sup> Y. Zhang and S. Das Sarma, *Phys. Rev. B* **72**, 075308 (2005).
  - <sup>40</sup> G. F. Giuliani and G. Vignale, *Quantum Theory of the Electron Liquid* (Cambridge, 2005).
  - <sup>41</sup> W. L. McMillan, *Phys. Rev.* **167**, 331 (1968).
  - <sup>42</sup> P. B. Allen and R. C. Dynes, *Phys. Rev. B* **12**, 905 (1975).